Accepted Manuscript

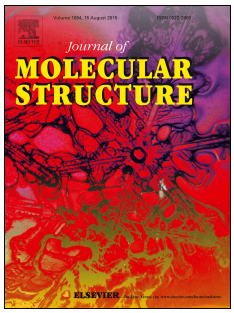

Tridentate Schiff base coordinated trigonal bipyramidal / square pyramidal copper(II) complexes: Synthesis, crystal structure, DFT / TD-DFT calculation, catecholase activity and DNA binding

Apurba Bhunia, Pavel Vojtíšek, Valerio Bertolasi, Subal Chandra Manna

PII: S0022-2860(19)30385-0

DOI: https://doi.org/10.1016/j.molstruc.2019.03.098

Reference: MOLSTR 26367

To appear in: *Journal of Molecular Structure*

Received Date: 11 October 2018

Revised Date: 1 March 2019

Accepted Date: 29 March 2019

Please cite this article as: A. Bhunia, P. Vojtíšek, V. Bertolasi, S. Chandra Manna, Tridentate Schiff base coordinated trigonal bipyramidal / square pyramidal copper(II) complexes: Synthesis, crystal structure, DFT / TD-DFT calculation, catecholase activity and DNA binding, *Journal of Molecular Structure* (2019), doi: https://doi.org/10.1016/j.molstruc.2019.03.098.

Graphical abstract

Tridentate Schiff base coordinated trigonal bipyramidal / square pyramidal copper(II) complexes: Synthesis, crystal structure, DFT / TD-DFT calculation, catecholase activity and DNA binding

Apurba Bhunia, Pavel Vojtíšek, Valerio Bertolasi, Subal Chandra Manna*

Using tridentate Schiff bases and 1,10-phenanthroline, complexes {[Cu(L^1)(phen)][Cu(L^1)(phen)]·5H_2O} (**1**) and {[Cu(L^2)(phen)](ClO_4)} (**2**) (H_2L^1 = 3-[(2-hydroxy-benzylidene)-amino]-propionic acid, HL^2 = 2-methoxy-6-[(3-methylamino-propylimino)-methyl]-phenol, phen = 1,10-phenanthroline) have been synthesized and structurally characterized. Complex **1** is a cocrystal with mononuclear trigonal bipyramidal and square pyramidal geometries. Spectroscopic study reveals that both the complexes show catecholase activity, and the complexes interact with the CT-DNA. Results of DFT and TD-DFT calculations are used to explain the structures and electronic spectral properties of the complexes.

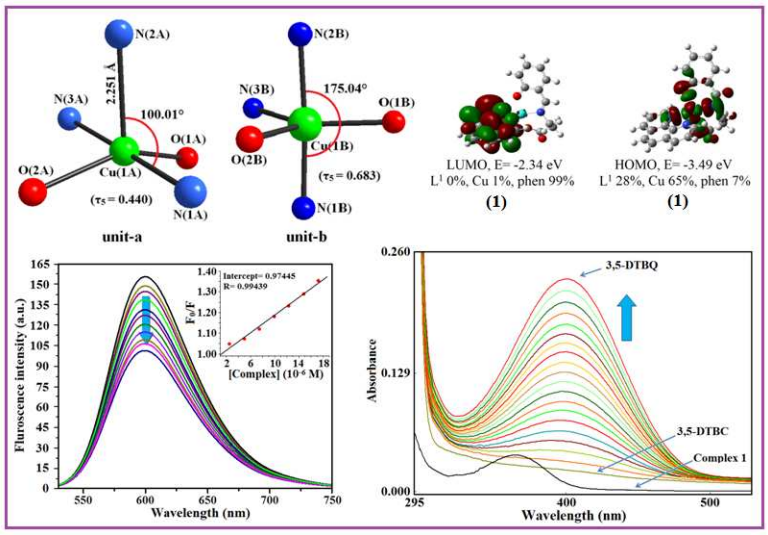

Tridentate Schiff base coordinated trigonal bipyramidal / square pyramidal copper(II) complexes: Synthesis, crystal structure, DFT / TD-DFT calculation, catecholase activity and DNA binding

Apurba Bhunia,[a] Pavel Vojtíšek,[b] Valerio Bertolasi,[c] Subal Chandra Manna*,[a]

[a]*Department of Chemistry and Chemical Technology, Vidyasagar University, Midnapore 721102, West Bengal, India, E-mail: scmanna@mail.vidyasagar.ac.in, Fax: (91) (03222) 275329.*

[b]*Department of Inorganic Chemistry, Charles University in Prague, Hlavova 2030/8, 128 43 Prague 2, Czech Republic.*

[c]*Dipartimento di Scienze Chimiche e Farmaceutiche, Centro di Strutturistica Diffrattometrica, Università di Ferrara, Via L. Borsari, 46, 44100 Ferrara, Italy.*

Abstract

Using tridentate O,N,O / N,N,O donor Schiff bases and 1,10-phenanthroline, five coordinated copper(II) complexes, {[Cu(L^1)(phen)][Cu(L^1)(phen)]·5H_2O}(**1**) and {[Cu(L^2)(phen)](ClO_4)}(**2**) [H_2L^1 = 3-[(2-hydroxy-benzylidene)-amino]-propionic acid, HL^2 = 2-methoxy-6-[(3-methylamino-propylimino)-methyl]-phenol, phen = 1,10-phenanthroline] have been synthesized and structurally characterized. Complex **1** is a co-crystal, where two geometrically different (trigonal bipyramidal (TBP) and square pyramidal (SP)) complexes of same compositions [Cu(L^1)(phen)] are within a unit cell. Complex **2** exhibits a trigonal bipyramidal geometry and counter balanced by perchlorate anion. In solid state, complex **1** contains both SP and TBP geometries, but theoretical calculation reveals that in solution it exists only in one form with SP geometry. DFT/TD-DFT calculations for the complexes were

performed to explain the structures and electronic spectral properties of the complexes. Both the complexes are active for catalytic oxidation of 3,5-di-*tert*-butylcatechol (3,5-DTBC) to 3,5-di-*tert*-butylquinone (3,5-DTBQ) in presence of molecular oxygen and the calculated values of turnover numbers are 62±3 and 52±3 h^{-1} for **1** and **2**, respectively. Interactions of complexes with calf thymus-DNA have been studied using fluorescence spectroscopic techniques and the calculated values of binding constants are (2.20±0.06) × 10^4 and (2.27±0.07) × 10^4 L mol^{-1} for complexes **1** and **2**, respectively.

Keywords: Copper(II) complexes; Cocrystal; Crystal structure; DFT/TD-DFT calculation; DNA binding.

1. Introduction

Chelating ligand based copper complexes are important for their potential applications in catalysis and biological activities [1]. Due to versatile coordination number copper can easily coordinate with the donor sites of organic ligands and form coordination complexes of various geometries [2-3]. Use of flexidentate chelating ligand and chelating pyridinyl ligand is an important strategy for designing mononuclear copper complexes. 1,10-phenanthroline is an important chelating ligand and behaves as a potential σ-donor and π-acceptor ligand [4], and due to extensive π character, it can form supramolecular connections with bio-molecules with π···π and CH···π interactions.

Cocrystals are single phase crystalline materials composed of two or more different molecules or ions in a stoichiometric ratio [5], and the cocrystals are important for their interesting physical and chemical properties and potential applications as pharmaceuticals, nonlinear optical materials and charge-transfer solids [6-7].

Catechol oxidase is an enzyme in plant system which catalyzes the oxidation process of *o*-diphenols to *o*-benzoquinones in presence of molecular oxygen. Active site of this metaloprotein contains two copper(II) centers [8]. It is interesting to note that in aerobic condition many copper(II)-Schiff base complexes mimic the catecholase activity [9].

The interaction of DNA with copper(II) complexes have been studied broadly in the field of biology and medicinal chemistry [10]. The complexes can interact with DNA and hence change the replication of DNA. Literature study show that copper complexes interact strongly with DNA molecules [11]. Metal complexes can interact with DNA molecules through covalently or non-covalently. Generally DNA bonded metal complexes are stabilized through the weak interactions with the base pairs of DNA which is known as intercalation. In addition to the interaction, the complexes may also bind with the DNA through groove binding mode and with electrostatic interactions [12]. Literature survey reveals that the magnitude and the mode of interaction of complexes with CT-DNA depend on the nuclearity and the geometry of the complexes, and on the choice of chelating ligands. Studies of the interaction of CT-DNA with new copper (II) complexes are important to get better understanding about the kinetics of interaction of complexes with CT-DNA. In the present study we have used O,N,O and N,N,O donor chelating ligands, 3-[(2-hydroxy-benzylidene)-amino]-propionic acid (H_2L^1) and 2-methoxy-6-[(3-methylamino-propylimino)-methyl]-phenol (HL^2), respectively, and synthesized two mononuclear Cu(II) complexes {[$Cu(L^1)$(phen)][$Cu(L^1)$(phen)]·$5H_2O$} (**1**) and {[$Cu(L^2)$(phen)](ClO_4)}(**2**). DFT/TD-DFT calculations have been performed to explain structure and electronic spectral properties of the complexes. Catecholase activity and CT-DNA interactions studies have also been performed using spectroscopic techniques.

2. Experimental

2.1. Materials

N-methyl-1,3-diaminopropane, 1,10-phenanthroline, calf thymus DNA, ethidium bromide, and 3,5-di-tertbutylcatechol were purchased from Aldrich chemical company. All other chemicals are of AR grade.

2.2. Physical measurements

Elemental analyses were performed using a Perkin-Elmer 240C elemental analyzer. IR spectra were recorded as KBr pellets on a Bruker Vector 22 FT IR spectrophotometer operating from 400 to 4000 cm^{-1}. Electronic absorption spectra were obtained with Shimadzu UV-1601 UV-vis spectrophotometer at room temperature. Emission spectra were recorded on Hitachi F-7000 spectrofluorimeter at room temperature. The fluorescence quantum yield [13] was determined using phenol as a reference in water [refractive index (η), 1.333)] and complexes inmethanol (η, 1.329). ESI mass spectra of complexes were determined using their methanolic and aqueous solutions (Acq. method: Direct Infusion_HPLC.m, Stream name: LC1, Acquisition SW Version: 6200 series TOF/6500 series Q-TOF B.08.00 (B8058.0), QTOF Driver Version: 8.00.00, QTOF Firmware Version: 20.698, Tune Mass Range Max.: 3200).

*2.3. Synthesis of {[Cu(L^1)(phen)][Cu(L^1)(phen)]·5H_2O} (**1**)*

The tridentate Schiff base (H_2L^1) was prepared by refluxing 2-hydroxybenzaldehyde (1 mmol, 0.122 g) and beta-alanine (1 mmol, 0.089 g) in methanol (15 mL) according to literature method [14]. An aqueous solution (10 mL) of copper perchlorate hexahydrate (1 mmol, 0.370 g) was added to the methanolic solution of mixture of triethylamine (2 mmol, 0.202 g) and H_2L^1 (1 mmol, 0.193 g) under stirring condition. To this reaction mixture a

methanolic solution (5 mL) of 1,10-phenanthroline (1 mmol, 0.180 g) was added drop wish and resulting green color reaction mixture was stirred for 2 h and filtered. The filtrate was kept in refrigerator for slow evaporation. After a few days green single crystals suitable for X-ray diffraction were obtained from the filtrate. Yield 0.408 g (85%). Anal. Calcd for $C_{44}H_{44}Cu_2N_6O_{11}$ (959.93): C, 55.05; H, 4.62; N, 8.75 %. Found: C, 55.03; H, 4.61; N, 8.77 (%). IR (cm^{-1}): 3100-3600(br, vs), 2943(s), 2887(s), 1656(vs), 1637(vs), 1553(vs), 1468(w), 1414(s), 1375(s), 1300(s), 1077(s), 880(s), 812(s), 634(s).

*2.4. Synthesis of {[Cu(L^2)(1,10-phen)](ClO$_4$)} (**2**)*

The Schiff base HL^2 was prepared by refluxing 2-hydroxy-3-methoxybenzaldehyde (1 mmol, 0.152 g) and N-methyl-1,3-diaminopropane (1 mmol, 0.088 g) in methanol (15 mL) according to literature method [14]. Complex **2** was synthesized adopting the same reaction procedure as for **1** using HL^2 (1 mmol, 0.222 g) instead of H_2L^1 and here 1 mmol (0.101 g) triethylamine used. Yield 0.4g (71 %). Anal. Calcd for $C_{24}H_{25}CuN_4O_6Cl$ (564.47): C, 51.06; H, 4.46; N, 9.92 %. Found: C, 51.08; H, 4.49; N, 9.90 (%). IR (cm^{-1}): 2985(s), 2945(s), 2886(s), 1638(vs), 1551(vs), 1542(vs), 1467(w), 1415(s), 1376(s), 1300(s), 1080(s), 881(s), 814(s), 637(s).

2.5. Crystallographic data collection and refinement

Data collection of complex **1** was carried out by using a Nonius Kappa CCD diffractometer with graphite monochromated Mo-Kα radiation, at room temperature. The data sets were integrated with the Denzo-SMN package [15] and corrected for Lorentz, polarization and absorption effects (SORTAV) [16]. The crystal data of complex **2** was collected on a Bruker APEX CCD diffractometer using graphite monochromated Mo-Kα radiation (λ = 0.7107 Å)

at 150 K [17]. The structure of the complexes were solved by direct methods SIR97 [18] and refined by full-matrix least squares methods with SHEL-XTL [19] with all non-hydrogen atoms anisotropically and both C-H and N-H hydrogens included on calculated positions, riding on their carrier atoms. In the final Difference Fourier mapsof complex **1,** ill-defined regions of residual eletron density were found not localized close to the water Oxygens. Accordingly, it was not possible to identify any hydrogen atom bonded to these Oxygens. The final geometrical calculations and graphical manipulations were carried out with the SHEL-XTL package [19]. All calculations were performed using SHELXL-97 [20] and PARST [21] implemented in WINGX [22] system of programs. Crystal data and details of refinements are given in Table 1. ORTEP views are shown in Figs. 1 and 2.

2.6. Theory and computational methods

Theoretical calculations were performed using the Gaussian 09 software package [23]. For the calculation 6-31G (d-p) basis set was used for the optimization of all elements, except copper atoms, for which the Los Alamos effective core potentials plus the Double Zeta (LanL2DZ) [24] basis set was employed. The geometric structures of the complexes in the ground state (doublet) were fully optimized by using the Becke's three-parameter hybrid exchange functional and the Lee-Yang-Parr non-local correlation functional (B3LYP) [25]. Electronic excitations based on B3LYP functional were obtained with the time-dependent density functional theory (TD-DFT) [26] in methanol using the conductor-like polarizable continuum model (CPCM) [27]. GaussSum [28] was used to calculate the fractional contributions of various groups to each molecular orbital.

2.7. DNA binding studies

Stock solutions of complexes and CT-DNA were prepared in HEPES buffer solution (pH 7.2). The competitive binding nature of ethidium bromide (EtBr) and complexes with CT-DNA were investigated adopting fluorometric method, using aqueous solution of CT-DNA bounded EtBr in HEPES buffer at room temperature. In presence of CT-DNA, ethidium bromide (EtBr) exhibits fluorescence enhancement due to its intercalative binding to CT-DNA. Competitive binding of complexes with CT-DNA results fluorescence quenching due to displacement of EtBr from CT-DNA molecules. The fluorescence intensities at 600 nm (λ_{ex}, 500 nm) of CT-DNA bounded EtBr with increasing concentration of complexes were recorded. The quenching constants (Stern-Volmer constant, K_{sv}) were calculated using Stern-Volmer equation [29]. Concentration of CT-DNA was determined [30] by measuring the absorbance (A) of CT-DNA solution at 260 nm and applying Lambert-Beer law [$A = \epsilon cl$, where A is the absorbance at 260 nm (characteristic band of CT-DNA), ϵ is the molar extinction coefficient 6600 L $mol^{-1}cm^{-1}$ per nucleotide, l is the path length of the beam of light through the sample (aqueous solution of CT-DNA), c is the molar concentration of CT-DNA.

3. Results and discussion

3.1. Crystal structure description

Solid state structure analysis of **1** and **2** show that both the compounds are five coordinated, mononuclear Cu(II) complexes. Complex **1** contains two geometrically different molecules and five lattice water molecules in the asymmetric unit. Molecular structure of complex **1** is shown in Fig.1. In complex **1** there are two five coordinated complex units (**unit-a** and **unit-b**). Complex **2** is a cationic complex and counter balanced by perchlorate anion (Fig. 2). The trigonality τ_5 parameter [31] calculation indicate that in **1**, the **unit-a** possesses distorted square pyramidal geometry (τ_5, 0.440), whereas **unit-b** possesses trigonal bipyramidal

geometry (τ_5,0.683) (Table 2). Calculated value of τ_5 for **2** is 0.732 indicating that the Cu(II) centre possesses distorted trigonal bipyramidal geometry (Table 3).

In **unit-a** of **1**, the N(2A) atom occupy the apical position with Cu(1A)-N(2A) bond distance 2.251Å, and O(1A), O(2A), N(1A), N(3A) atoms form basal plane. Whereas in **unit-b** O(1B), O(2B), N(3B) atoms form trigonal plane, and N(1B) and N(2B) atoms occupy apical position with N(1B)-Cu(1B)-N(2B) bond angle as 175.04(15)° (Table 2 and Fig. 3). Packing diagram of **1** shows that the alternate arrangement of **unit-a** and **unit-b**, and form 1D supramolecular chain through three different types of π···π interactions [Cg(7)···Cg(7)= 3.506Å, Cg(14)···Cg(15)= 3.672Å, Cg(14)···Cg(5)= 3.606Å] (Fig. 4). The 1D supramolecular chains are again linked through C-H···π interactions [H(20B)···Cg(6)= 2.707Å] and form 2D supramolecular sheet like structure (Fig. 1S and Table 1S).

Complex **2** exhibits trigonal bipyramidal geometry, where phenolic oxygen (O1), one Schiff base nitrogen (N2) and one nitrogen from phen (N4) form trigonal plane. The Schiff base nitrogen (N1) and nitrogen from phen (N3) placed at the opposite sides of the plane. In the trigonal plane the coordination bond distances fall in the ranges 1.929(13)Å-2.196(15)Å and N(1)-Cu(1)-N(3) is 176.24(7)° (Table 3). Packing diagram of **2** shows 2D supramolecular structure formed by π···π [Cg(4)···Cg(5)= 3.703 Å] and C-H···π [H(9B)···Cg(5)= 3.643Å] interactions (Fig. 5 and Table 2S).

3.2. ESI mass spectrometry

The ESI mass spectra of complexes were recorded in methanolic and aqueous solutions. For complex **1** the methanolic solution shows peak at m/z = 434.9404, whereas aqueous solution shows peak at m/z = 434.9347. These peaks corresponds to the presence of species $[Cu(L^1)(1,10\text{-phen})]^{+}$ (calc. m/z = 434.93) (Figs. 2S and 3S). For complex **2**, peaks are at 464.95 and 465.0014 in methanolic and aqueous medium, respectively, corresponding to the

complex cation $[Cu(L^2)(1,10\text{-phen})]^+$ (calc. m/z = 465.02). These observations clearly indicate that the complexes are stable in both methanol and water medium.

3.3. DFT / TD-DFT computations

Structure of the complexes were fully optimized at the B3LYP level in the ground state using LanL2DZ basic set and the optimized structures are depicted in Figs. 6S and 7S for **1** and **2**, respectively. A comparison of calculated bond lengths and angles with X-ray crystal structures shows sufficient agreement (Table 2 and 3). The orbital diagrams along with their energies and contributions from the ligands and metal of **1** and **2** are given in Figs 8S and 9S. HOMO and LUMO of complexes are mostly contributed from copper and phenanthroline respectively (Fig. 6a). HOMO-LUMO energy differences are 1.15 eV and 1.10 eV for **1** and **2**, respectively indicating that **1** is kinetically more stable in comparison to **2**. A comparative MOs energy level diagrams are depicted in Fig. 6b.

In the solid state structure **1** possesses two units with square pyramidal (**unit-a**) and trigonal bipyramidal (**unit-b**) geometries. Calculated energies of **unit-a** and **unit-b** are -39027.958191983 eV and -39027.867335077 eV, respectively. It is interesting to note that when both **unit-a** and **unit-b** are optimized in methanol adopting CPCM model, both the units finally maintain square pyramidal geometry, which corroborates the higher stability of square pyramidal geometry.

TD-DFT calculations of complexes in methanol using conductor-like polarizable continuum model (CPCM) were performed. Theoretically possible spin-allowed electronic transitions with their assignment are listed in Tables 3S and 4S, for **1** and **2**, respectively. The TD-DFT results show that [HOMO-7(α) →LUMO+1(α) (20%), HOMO-7(β) →LUMO+2(β) (22%)] and [HOMO-6(β) →LUMO(β) (10%), HOMO-2(β) →LUMO(β) (12%), HOMO(β) →LUMO(β) (44%)] are the possible highest energy electronic transitions and lowest energy electronic transitions for **1**. For **2**, [HOMO-5(α) →LUMO+2(α) (31%)] and [HOMO-4(β)

→LUMO(β)(16%), HOMO(β) → LUMO(β)(62%)] are possible highest and lowest energy electronic transitions, respectively. For **1**, the experimental electronic transition at 267 nm is assigned as combination of intraligand charge transition in phen [HOMO-8(α) →LUMO+1(α) (30%), ILCT[§]] and interligand charge transfer transition from L^1 to phen [HOMO-6(α) →LUMO+1(α) (16%), IELCT[Γ]] (Table 4, Fig. 10S). For **2**, electronic transition at 260 nm is assigned as ligand to metal charge transfer transition from L^2 to copper [HOMO-6(β) → LUMO (β) (17%), LMCT[δ]] (Table 4, Fig. 11S).

3.4. Catechol oxidase studies of complexes

3,5-di-tertbutylcatechol (3,5-DTBC) was used as model substrate to examine the catecholase activity of the complexes at room temperature [32]. Catalytic amount of methanolic solution of (1×10^{-4} M) complexes were added to methanolic solution of 3,5-DTBC (1×10^{-2} M) and the progress of the reaction was determined by recording the absorbance at 400 nm (characteristic absorption band of 3,5-di-tertbutyl quinone). The absorbance of complex-substrate mixture gradually increases upon addition of complexes to the substrate (Figs. 7 and 12S). The rate constants for the formation of 3,5-di-tertbutyl quinone were obtained using the equation $\ln[A_\infty/(A_\infty - A_t)] = kt$ where A_∞ and A_t are the absorbance of 3,5-di-tertbutyl quinone at time $t = \infty$ and $t = t$, respectively [33]. Calculated values of rate constants are $1.2\pm0.02 \times 10^{-2}$ min^{-1} and $1.1\pm0.01 \times 10^{-2}$ min^{-1} for **1** and **2**, respectively (Fig. 13S).

To determine the dependence of rate of reaction on substrate concentration same experiment were carried out varying the substrate concentration from 1×10^{-3} M to 10×10^{-3} M. The reaction shows first order dependence at low concentration of substrate, but at higher concentration the saturation kinetics was observed (Fig. 8). As the catalytic reactions follow saturation kinetics, Michaelis–Menten kinetic approach has been used to evaluate kinetic parameters [34]. Calculated values of turnover number (K_{cat}) are 62±3 and 52±3 h^{-1},

respectively (Table 5). Complexes **1** and **2** show comparable catecholase activity with the reported Cu(II) complexes (Table 5).

3.5. DNA binding studies

Interactions of CT-DNA with metal complexes have been studied by monitoring the emission intensity of CT-DNA bounded ethidium bromide (EtBr). Emission intensity of ethidium bromide (EtBr) enhanced significantly in presence of CT-DNA due to the strong intercalation of EtBr with DNA [35]. On excitation at 500 nm, EtBr and CT-DNA mixture shows emission at 600 nm. Addition of a compound which is capable to interact with CT-DNA, results the quenching of fluorescence intensity. Upon gradual addition of 5µL 1 mM solution of complexes to the 2 mL CT-DNA bounded EtBr solution (mixture of 8.7 µM CT-DNA solution and 12 µM EtBr solution) results the reduction of fluorescence intensity of 600 nm band (Figs. 9 and 14S). Reduction of emission intensity clearly indicates that complexes **1** and **2** displaced the EtBr molecules from the DNA binding sites [36]. The calculated values of binding constants (K_{sv}) are $(2.20\pm0.06) \times 10^4$ and $(2.27\pm0.07) \times 10^4$ L mol^{-1} for complexes **1** and **2**, respectively (Table 6). A comparison of binding constants for reported Cu(II) complexes and shown in Table 6 and from this table it is clear that the complexes **1** and **2** have comparable interaction abilities with those of reported Cu(II) complexes.

4. Conclusion

In the present contribution we report synthesis, crystal structure, DFT calculation, catecholase activity and DNA binding studies of two five coordinated SP /TBP copper(II) complexes. Use of chelating H_2L^1 and phen ligands results complex **1**, where mononuclear copper(II) complexes of SP and TBP geometries are within the same unit cell. On the other hand use of HL^2 and phen results complex **2** of TBP geometry. Theoretical calculation reveals that in between SP (**unit-a**) and TBP (**unit-b**) units in **1**, the SP unit is energetically more stable. The

optimization of geometries of **unit-a** and **unit-b** adopting CPCM model (in methanol) results SP geometries for both the units, which corroborates with less energetic conformation of five coordinate SP geometry in **1**. On the other hand DFT calculation reveals that **2** maintains its TBP geometry in its methanolic solution also. The results of TD-DFT calculation have been used to explain the structure and electronic spectral properties of the complexes. UV-vis spectral study indicates that both the complexes are active for catalytic oxidation of 3,5-DTBC to 3,5-DTBQ. Fluorescence spectroscopic studies evidence that both complexes interact with CT-DNA.

Acknowledgements

The authors gratefully acknowledge the financial assistance given by the CSIR, Government of India, to Dr. Subal Chandra Manna (project no. 01 (2743)/13/EMR ‑ II). Authors thank UGC ‑ SAP, DST ‑ FIST New Delhi, USIC (VU) and Vidyasagar University for infrastructural facilities.

Supplementary information

Crystallographic data have been deposited at the Cambridge Crystallographic Data Centre and allocated the deposition numbers are CCDC 1847953 and 1847954. These data can be obtained free of charge via www.ccdc.cam.ac.uk/conts/retrieving.html or on application to CCDC, Union Road, Cambridge, CB2 1EZ, UK [fax: (+44)1223-336033, e-mail: deposit@ccdc.cam.ac.uk].

X-ray crystallographic data, electronic absorption spectra, emission spectra, IR spectra, ESI mass spectra and results of DFT calculation are provided as supplementary material.

References

[1] (a) P. Kumar, S. Gorai, M.K. Santra, B. Mondal, D. Manna, Dalton Trans.41 (2012) 7573–7581; (b) M. Zampakou, S. Balala, F. Perdih, S. Kalogiannis, I. Turelc, G. Psomas, RSC Adv. 5(2015) 11861–11872; (c) S. Mistri, A. Paul, A. Bhunia, R.K. Manne, M.K. Santra, H. Puschmann, S.C. Manna, Polyhedron 104 (2016) 63-72; (d) S. Mistri, V. Bertolasi, S.C. Manna, Polyhedron 88 (2015) 101-109.

[2] (a) A. Paul, V. Bertolasi, A. Figuerola, S.C. Manna, J. Solid State Chem. 249 (2017) 29-38; (b) K. Fujisawa, Y. Noguchi, Y. Miyashita, K.-I. Okamoto, N. Lehnert, Inorg. Chem. 46 (2007) 10607-10623.

[3] (a) S. Kathiresan, S. Mugesh, M. Murugan, F. Ahamed, J. Annaraj, RSC Adv. 6 (2016) 1810-1825; (b) N. Biswas, S. Khanra, A. Sarkar, S. Bhattacharjee, D.P. Mandal, A. Chaudhuri, S. Chakraborty, C.R. Choudhury, New J. Chem. 41 (2017) 12996-13011; (c) S.C. Manna, S. Manna, A. Paul, E. Zangrando, A. Figuerola, S. Dolai, K. Das, ChemistrySelect 2 (2017) 3317-3322.

[4] (a) P.G. Sammes, G. Yahioglu, Chem. Soc. Rev. 23 (1994) 327–334; (b) G. Chelucci, A. Saba, G. Sanna, F. Soccolini, Tetrahedron: Asymmetry 11 (2000) 3427-3438; (c) E. Schoffers, Eur. J. Org. Chem. 2003, 1145–1152.

[5] (a) E. Grothe, H. Meekes, E. Vlieg, J.H. ter Horst, R. de Gelder, Cryst. GrowthDes. 16 (2016) 3237-3243; (b) S. Tothadi, P. Sanphui, G.R. Desiraju, Cryst. Growth Des. 14 (2014) 5293-5302.

[6] (a) O. Almarsson, M. Zaworotko, J. Chem. Commun. (2004)1889-1896; (b) M. Morimoto, M. Irie, J. Am. Chem. Soc. 32 (2010) 14172-14178; (c) T. Ono, M. Sugimoto, Y. Hisaeda, J. Am. Chem. Soc. 137 (2015) 9519-9522.

[7] (a) M. Nayak, R. Koner, H.H. Lin, U. Florke, H.H. Wei, S. Mohanta, Inorg. Chem. 45 (2006) 10764–10773; (b) S. Hazra, R. Koner, M. Nayak, H.A. Sparkes, J.A.K. Howard, S.

Mohanta, Cryst. Growth Des. 9 (2009) 3603–3608; (c) S. Sarkar, M. Nayak, M. Fleck, U. Florke, S. Dutta, R. Koner, S. Mohanta, Eur. J. Inorg. Chem. (2010) 735-743.

[8] (a) E.I. Solomon, M.J. Baldwin, M.D. Lowery, Chem. Rev. 92 (1992) 521-542; (b) N. Kitajima, Y. Moro-Oka, Chem. Rev. 94 (1994) 737-757.

[9] (a) S. Kumari, A.K. Mahato, A. Maurya, V.K. Singh, N. Kesharwani, P. Kachhap, I.O. Koshevoy, C. Haldar, New J. Chem. 41 (2017) 13625-13646; (b) T.P. Camargo, R.A. Peralta, R. Moreira, E.E. Castellano, A.J. Bortoluzzi, A. Neves, Inorg. Chem. Commun. 37 (2013) 34-38; (c) A. Neves, L.M. Rossi, A.J. Bortoluzzi, B. Szpoganicz, C. Wiezbicki, E. Schwingel, Inorg. Chem. 41 (2002) 1788-1794; (d) R.E.H.M.B. Osorio, R.A. Peralta, A.J. Bortoluzzi, V.R. de Almeida, B. Szpoganicz, F.L. Fischer, H. Terenzi, A.S. Mangrich, K.M. Mantovani, D.E.C. Ferreira, W.R. Rocha, W. Haase, Z. Tomkowicz, A. dos Anjos, A. Neves, Inorg. Chem. 51 (2012) 1569-1589; (e) A. Biswas, L.K. Das, M.G.B. Drew, C. Diaz, A. Ghosh, Inorg. Chem. 51 (2012) 10111-10121.

[10] (a) S.S. Bhat, A.A. Kumbhar, H. Heptullah, A.A. Khan, V.V. Gobre, S.P. Gejji, V.G. Puranik, Inorg. Chem. 50 (2011) 545-558; (b) D.S. Raja, N.S.P. Bhuvanesh, K. Natarajan, Inorg. Chem. 50 (2011) 12852-12866

[11] (a) A. Paul, S. Mistri, A. Bhunia, S. Manna, H. Puschmann, S.C. Manna, RSC Adv. 6 (2016) 60487-60501; (b) A. Paul, A. Figuerola, V. Bertolasi, S.C. Manna, Polyhedron 119 (2016) 460–470; (c) T.S. Mahapatra, A. Roy, S. Chaudhury, S. Dasgupta, S.L. Shrivastava, V. Bertolasi, D. Ray, Eur. J. Inorg. Chem. (2017) 769-779; (d) F. Arjmand, Z. Afsan, T. Roisnelb, RSC Adv. 8 (2018) 37375–37390; (e) R. Loganathan, S. Ramakrishnan, E. Suresh, A. Riyasdeen, M.A. Akbarsha, M. Palaniandavar, Inorg. Chem. 51 (2012) 5512−5532.

[12] (a) S.N. Kikandi, S. Musah, K. Lee, J. Hassani, S. Rajan, A. Zhou, O.A. Sadik, Electroanalysis 19 (2007) 2131 – 2140; (b) A.M. Pyle, J.P. Rehmann, R. Meshoyrer, C.V. Kumar, N.J. Turro, J.K. Barton, J. Am. Chem. Soc. 111 (1989) 3051-3058.

[13] J.R. Lakowicz, Principles of Fluorescence Spectroscopy, Third Edition, Springer, New York, USA, 2006.

[14] A. Bhunia, S. Manna, S. Mistri, A. Paul, R.K. Manne, M.K. Santra, V. Bertolasi, S.C. Manna, RSC Adv. 5 (2015) 67727-67737.

[15] Z. Otwinowski, W. Minor, Methods in Enzymology, Eds.: C.W. Carter, R.M. Sweet, Vol. 276, Part A, Academic Press, London, 1997, 307-326.

[16] R.H. Blessing, ActaCrystallogr. Sect A. 51 (1995) 33-38.

[17] Bruker 2000, SMART (Version 5.0), SAINT-plus (Version 6), and SADABS (Version 2.03); Bruker AXS Inc.: Madison, WI.

[18] A. Altomare, M.C. Burla, M. Camalli, G.L. Cascarano, C. Giacovazzo, A. Guagliardi, A. G. Moliterni, G. Polidori, R. Spagna, J. Appl. Crystallogr. 32 (1999) 115-118.

[19] G. M. Sheldrick, SHELXTL vesion 6.14, Bruker-AXS, Madison, W1, USA, 2003.

[20] G.M. Sheldrick, ActaCryst. A64 (2008) 112-122.

[21]M. Nardelli, J. Appl. Crystallogr. 28 (1995) 659.

[22] L.J. Farrugia, J. Appl. Crystallogr. 32 (1999) 837-838.

[23] Gaussian 09, revision A.02; Gaussian, Inc.: Wallingford, CT, 2009.

[24] P.J. Hay, W.R. Wadt, J. Chem. Phys. 82 (1985) 270-283.

[25] C. Lee, W. Yang, R.G. Parr, Phys. Rev. 37B (1988) 785-789.

[26] (a) R.E. Stratmann, G.E. Scuseria, M.J. Frisch, J. Chem. Phys. 109 (1998) 8218-8224; (b) M.E. Casida, C. Jamorski, K.C. Casida, D.R. Salahub, J. Chem. Phys. 108 (1998) 4439-4449.

[27] M. Cossi, N. Rega, G. Scalmani, V. Barone, J. Comput. Chem. 24(2003) 669-681.

[28] N.M. O'Boyle, A.L. Tenderholt, K.M. Langner, J. Comput. Chem.29 (2008) 839-845.

[29] (a) S. Veeralakshmi, S. Nehru, S. Arunachalam, P. Kumar, M. Govindaraju, Inorg. Chem. Front. 1 (2014) 393-404; (b) F.-F. Tian, J.-H. Li, F.-L. Jiang, X.-L. Han, C. Xiang, Y.-S. Ge, L.-L. Li, Y. Liu, RSC Adv. 2 (2012) 501-513.

[30] (a) S.S. Bhat, A.A. Kumbhar, H. Heptullah, A.A. Khan, V.V. Gobre, S.P. Gejji, V.G. Puranik, Inorg. Chem. 50 (2011) 545-558; (b) M.E. Reichmann, S.A. Rice, C.A. Thomas, P. Doty, J. Am. Chem. Soc. 76 (1954) 3047-3053.

[31] A.W. Addison, T.N. Rao, J. Reedijk, J.V. Rijn, G.C. Verschoor, J. Chem. Soc. Dalton Trans. (1984) 1349-1356.

[32] (a) P. Seth, L.K. Das, M.G.B. Drew, A. Ghosh, Eur. J. Inorg. Chem. 2012 (2012) 2232-2242; (b) P. Kar, R. Haldar, C.J. Gómez-García, A. Ghosh, Inorg. Chem. 51 (2012) 4265-4273.

[33] E. Monzani, L. Quinti, A. Perotti, L. Casella, M. Gullotti, L. Randaccio, S. Geremia, G. Nardin, P. Faleschini, G. Tabbı, Inorg. Chem. 37 (1998) 553-562.

[34] Enzyme Kinetics: Principles and Methods, 3rd edition. Hans Bisswanger, WILEY-VCH, (2017).

[35] P.U. Maheswari, M. Palaniandavar, J. Inorg. Biochem. 98 (2004) 219-230.

[36] (a) Z.-C. Liu, B.-D. Wang, B. Li, Q. Wang, Z.-Y. Yang, T.-R. Li, Y. Li, Eur. J. Med. Chem. 45 (2010) 5353-5361; (b) L. Tjioe, A. Meininger, T. Joshi, L. Spiccia, B. Graham, Inorg. Chem. 50 (2011) 4327-4339.

Table 1. Crystal data and details of structures refinement for complexes **1** and **2**.

Complex	**1**	**2**
Empirical formula	$C_{44}H_{44}Cu_2N_6O_{11}$	$C_{24}H_{25}CuN_4O_6Cl$
Formula mass, g mol^{-1}	959.93	564.47
Crystal system	Triclinic	Monoclinic
Space group	P-1	P21/n
a, Å	12.6179(6)	9.9833(3)
b, Å	12.6487(5)	18.2146(6)
c, Å	14.6636(5)	13.7179(5)
α, deg	79.457(3)	90
β, deg	86.278(2)	108.590(1)
γ, deg	68.199(2)	90
Z	2	4
V, Å^3	2136.24(16)	2364.34(14)
$D_{(calcd)}$, g cm^{-3}	1.477	1.586
μ(Mo-Ka), mm^{-1}	1.064	1.087
F(000)	972	1164
Theta range, deg	2.2, 27.0	1.9, 27.5
No. of collected data	27412	20194
No. of unique data	9265	5424
R_{int}	0.091	0.025
h,k,lmax	16, 16, 18	12, 22, 17
Observed reflections [$I > 2\sigma(I)$]	6493	4518
Goodness of fit (F^2)	1.065	1.047
Parameters refined	568	327
*R*1, *wR*2 (all data)[a]	0.0632, 0.1805	0.0312, 0.0828
Residuals, e Å^{-3}	-0.79, 0.76	-0.36, 0.41

[a] $R1(Fo) = \Sigma \big| |Fo| - |Fc| \big| / \Sigma |Fo|$, $wR2(Fo^2) = [\Sigma w (Fo^2 - Fc^2)^2 / \Sigma w (Fo^2)^2]^{½}$

Table 2. Experimental and calculated[α] coordination bond lengths (Å) and angles (°) for **1**.

Unit-a	Exp	Unit-b	Exp	Calcd
Cu(1A)-O(1A)	1.933(2)	Cu(1B)-O(1B)	1.936(3)	1.974
Cu(1A)-O(2A)	1.981(4)	Cu(1B)-O(2B)	2.145(3)	2.017
Cu(1A)-N(1A)	1.938(3)	Cu(1B)-N(1B)	1.947(4)	1.978
Cu(1A)-N(2A)	2.251(4)	Cu(1B)-N(2B)	2.000(3)	2.313
Cu(1A)-N(3A)	2.020(3)	Cu(1B)-N(3B)	2.118(3)	2.052
O(1A)-Cu(1A)-O(2A)	149.26(13)	O(1B)-Cu(1B)-O(2B)	112.34(12)	153.77
O(1A)-Cu(1A)-N(1A)	93.76(13)	O(1B)-Cu(1B)-N(1B)	93.21(14)	92.37
O(1A)-Cu(1A)-N(2A)	106.41(13)	O(1B)-Cu(1B)-N(2B)	91.03(14)	104.56
O(1A)-Cu(1A)-N(3A)	90.54(13)	O(1B)-Cu(1B)-N(3B)	134.01(14)	88.28
O(2A)-Cu(1A)-N(1A)	91.23(14)	O(2B)-Cu(1B)-N(1B)	88.76(13)	92.41
O(2A)-Cu(1A)-N(2A)	102.53(15)	O(2B)-Cu(1B)-N(2B)	92.00(13)	99.75
O(2A)-Cu(1A)-N(3A)	85.30(14)	O(2B)-Cu(1B)-N(3B)	113.05(13)	87.34
N(1A)-Cu(1A)-N(2A)	100.01(14)	N(1B)-Cu(1B)-N(2B)	175.04(15)	101.18
N(1A)-Cu(1A)-N(3A)	175.69(15)	N(1B)-Cu(1B)-N(3B)	94.78(14)	178.95
N(2A)-Cu(1A)-N(3A)	78.31(13)	N(2B)-Cu(1B)-N(3B)	80.41(14)	77.85
τ_5 parameter	0.440		0.683	0.419

[α]Using conductor-like polarizable continuum model (CPCM) in methanol; basis set, LanL2DZ; B3LYP functional.

Table 3. Experimental and calculated[α] coordination bond lengths (Å) and angles (°) for **2**.

	Exp	Calcd
Cu(1)-O(1)	1.929(13)	1.985
Cu(1)-N(1)	1.952(17)	1.995
Cu(1)-N(2)	2.127(17)	2.125
Cu(1)-N(3)	2.029(16)	2.072
Cu(1)-N(4)	2.196(15)	2.286
O(1)-Cu(1)-N(1)	92.73(6)	92.27
O(1)-Cu(1)-N(2)	129.66(6)	141.88
O(1)-Cu(1)-N(3)	88.13(6)	87.54
O(1)-Cu(1)-N(4)	132.28(6)	108.4
N(1)-Cu(1)-N(2)	93.81(7)	92.60
N(1)-Cu(1)-N(3)	176.24(7)	177.03
N(1)-Cu(1)-N(4)	98.01(6)	99.32
N(2)-Cu(1)-N(3)	88.45(6)	89.35
N(2)-Cu(1)-N(4)	95.95(6)	107.98
N(3)-Cu(1)-N(4)	78.75(6)	77.93
τ_5 parameter	0.732	0.585

[α]Using conductor-like polarizable continuum model (CPCM) in methanol; basis set, LanL2DZ; B3LYP functional.

Table 4. Selected UV-Vis energy transition at the TD-DFT[α]/B3LYP level for **1** and **2** in methanol.

Complex	λ_{exp} (nm), ε_{exp} ($M^{-1}cm^{-1}$)	λ_{cal} (nm), ε_{cal} ($M^{-1}cm^{-1}$)	Oscillator strength	Key transition	Character[b]
1	266, 8.57×10^4	267.08, 29615	0.1039	HOMO-8(α) →LUMO+1(α) (30%), HOMO-6(α) →LUMO+1(α) (16%)	ILCT[§] IELCT[Γ]
		267.45, 29667	0.1663	HOMO-8(α) →LUMO+1(α) (17%)	ILCT[§]
2	263, 6.97×10^4	260.51, 58054	0.0289	HOMO-6(β) →LUMO (β) (17%)	LMCT[δ]
		265.34, 53712	0.0804	HOMO-4(α) →LUMO+1(α) (29%), HOMO-5(β) →LUMO+2(β) (27%)	ILCT[§] ILCT[§]

[α]Using conductor-like polarizable continuum model (CPCM) in methanol; basis set, LanL2DZ.

[b]ILCT[§]= Intra ligand charge transfer of phen, IELCT[Γ]= Inter ligand charge transfer from L^1 to phen, LMCT[δ]= Charge transfer transition from L^2 to copper.

Table 5. Kinetic parameters for the oxidation of 3,5-DTBC catalyzed by Cu(II) complexes.

Complex	V_{max} ($M\ min^{-1}$)	Fitting error	K_m (M)	Fitting error	K_{cat} (h^{-1})	Fitting error	ref
1	3.4×10^{-5}	$\pm 0.4 \times 10^{-5}$	2.4×10^{-3}	$\pm 0.002 \times 10^{-3}$	62	± 3	This work
2	2.8×10^{-5}	$\pm 0.5 \times 10^{-5}$	2.3×10^{-3}	$\pm 0.002 \times 10^{-3}$	52	± 3	This work
$[Cu(sal\text{-}ppzH)Cl_2]$	9.85×10^{-6}		5.3×10^{-3}		11.82		[9(a)]
$[Cu(hyap\text{-}ppzH)Cl_2]$	2.38×10^{-5}		4.2×10^{-3}		28.80		[9(a)]
$Cu(H_2LDA)(ClO_4)](ClO_4)$	-		3.5×10^{-3}		58.68		[9(b)]
$[Cu_2(H_2\text{-}bbppnol)\text{-}(\mu\text{-}OAc)(H_2O)_2]Cl_2,2H_2O$	1.14×10^{-5}		7.9×10^{-4}		28.44		[9(c)]
$[Cu_2(Hbtppnol)(\mu\text{-}OAc)](ClO_4)$	1.14×10^{-5}		9.5×10^{-4}		28.08		[9(c)]
$[Cu_2(P1\text{-}O\text{-})(OAc\text{-})](ClO_4)_2$	4.02×10^{-6}		8.6×10^{-4}		10.08		[9(c)]
$[Cu_2(L^1)(\mu\text{-}OAc)]\text{-}(ClO_4)_2\cdot(CH_3)_2CHOH$	3.70×10^{-5}		3.47×10^{-3}		90		[9(d)]
$[Cu_2(L^2)\text{-}(\mu\text{-}OAc)]\text{-}(ClO_4)\cdot H2O\cdot(CH_3)_2CHOH$	7.44×10^{-5}		9.44×10^{-3}		183.6		[9(d)]
$[Cu_2(L^3)(\mu{-}OAc)]^{2+}$	1.14×10^{-5}		9.50×10^{-4}		28.08		[9(d)]
$[Cu_2L^4(ClO4)_2]$	1.56×10^{-4}		3.32×10^{-3}		93.6		[9(e)]
$[Cu_2L^4(OH)]ClO_4$	3.89×10^{-4}		4.60×10^{-3}		233.4		[9(e)]

Hsal-ppz and Hyap-ppz are derived by reacting 1-(2-aminoethyl) piperazine with salicylaldehyde and 2-hydroxyacetophenone, respectively. H_2LDA = N,N′-[bis-(2-hydroxy-3-formyl-5-methylbenzyl)(dimethyl)]-ethylenediamine, H_3bbppnol= N,N′-bis(2-hydroxybenzyl)-N,N′-bis- (pyridylmethyl)]-2-hydroxy-1,3-propanediamine, H2btppnol= N-(2-hydroxybenzyl)-N,N′,N′-tris(2-pyridylmethyl)-1,3-diaminopropan2-ol, P1-OH= 1,3-bis[bis(2-pyridylmethyl)amino]propanolate, L^1= N′,N′, N-tris(2-pyridylmethyl)-N-(2-hydroxy-3,5-di-tert-butylbenzyl)- 1,3-propanediamin-2-ol, L^2= N′,N′-bis(2-pyridylmethyl)-N,N-(2-hydroxybenzyl)(2-hydroxy-3,5-di-tert-butylbenzyl)- 1,3-propanediamin-2-ol, L^3 = N-(2-hydroxybenzyl)-N′,N′,N-tris(2-pyridylmethyl)-1,3-propanediamin-2-ol, HL^4= 2-[[2-(diethylamino)-ethylamino]methyl]phenol.

Table 6. Kinetic parameter for the interactions of Cu(II) complexes with CT-DNA.

Complex	K_{sv} (L mol^{-1})	Fitting error	ref
1	2.20×10^4	$\pm 0.06 \times 10^4$	This work
2	2.27×10^4	$\pm 0.07 \times 10^4$	This work
$[Cu(L^1)(pa)]$	1.40×10^5		[11(a)]
$[Cu(L^1)(mb)]$	1.99×10^5		[11(a)]
$\{[Cu_2(L^2)_2(fum)](H_2O)(MeOH)\}_n$	1.71×10^5		[11(b)]
$[Cu_4(\mu\text{-}L^3)_2(\mu_{1,1,3,3}\text{-}O_2CH)](OH)_6H_2O$	4.73×10^4		[11(c)]
$[Cu(L^4)(phen)(NO_3)]$	6.12×10^4		[11(d)]
$[Cu(L^4)(bpy)(NO_3)]$	3.80×10^4		[11(d)]
$[Cu(L^4)(DACH)(NO_3)]$	4.68×10^4		[11(d)]
$[Cu(bba)(bpy))]^{2+}$	1.7×10^5		[11(e)]
$[Cu(bba)(phen)]^{2+}$	3.6×10^5		[11(e)]
$[Cu(bba)(5,6\text{-}dmp)]^{2+}$	1.08×10^6		[11(e)]
$[Cu(bba)(dpq)]^{2+}$	5.1×10^5		[11(e)]

HL^1= o-{(3-morpholinopropylimino)methyl}phenol, pa= 3-phenylacrylate, mb= p-methylbenzoate, fum= fumarate, Schiff base (HL^2) derived from the condensation reaction of 2-amino-1-butanol and salicylaldehyde. H_3L^3 = 1,3-bis [3-aza-3-(1-methyl-3-oxobut-1-enyl)prop-3-en-1-yl]-2-(2-hydroxyphenyl)-1,3-imidazolidine, L^4= 3-formylchromone, phen= 1,10-phenanthroline, bpy= 2,2′-bipyridine, DACH= 1R,2R-DACH, bba= N,N-bis(benzimidazol-2-ylmethyl)-amine, 5,6-dmp= 5,6-dimethyl-1,10-phenanthroline, dpq= dipyrido[3,2-d:2,3-f] quinoxaline.

Figure captions

Fig. 1. ORTEP view of complex **1** showing the thermal ellipsoids at 30% probability level.

Fig. 2. ORTEP view of complex **2** showing the thermal ellipsoids at 30% probability level.
Fig. 3. Square pyramidal and trigonal bipyramidal coordination arrangement Cu(II) centers in complex **1**.

Fig. 4. 1D Supramolecular structure of complex **1**.

Fig. 5. 2D Supramolecular structure of complex **2**.

Fig. 6. (a) Surface plots of HOMO and LUMO for complexes **1** and **2** (with energies and compositions). (b) Molecular orbital energy level diagrams for **1** and **2**.

Fig. 7. Absorbance *vs* time plot for the oxidation of 3,5-di-*tert*-butylquinone (3,5-DTBQ)

catalyzed by complex **1**.

The spectra were recorded at an interval of 5 min.

Fig. 8. (a) Plots of rate *vs* substrate concentration, and (b) Lineweaver–Burk plots for complexes **1** and **2**.

Fig. 9. Fluorescence quenching curves of EtBr bounded CT-DNA upon gradual addition of 5 µL 1 mM solution of **1** to 2 mL aqueous solution of EtBr-CT-DNA (mixture of 8.7 µM CT-DNA solution and 12 µM EtBr solution) (inset: Stern-Volmer plot for fluorescence titration).

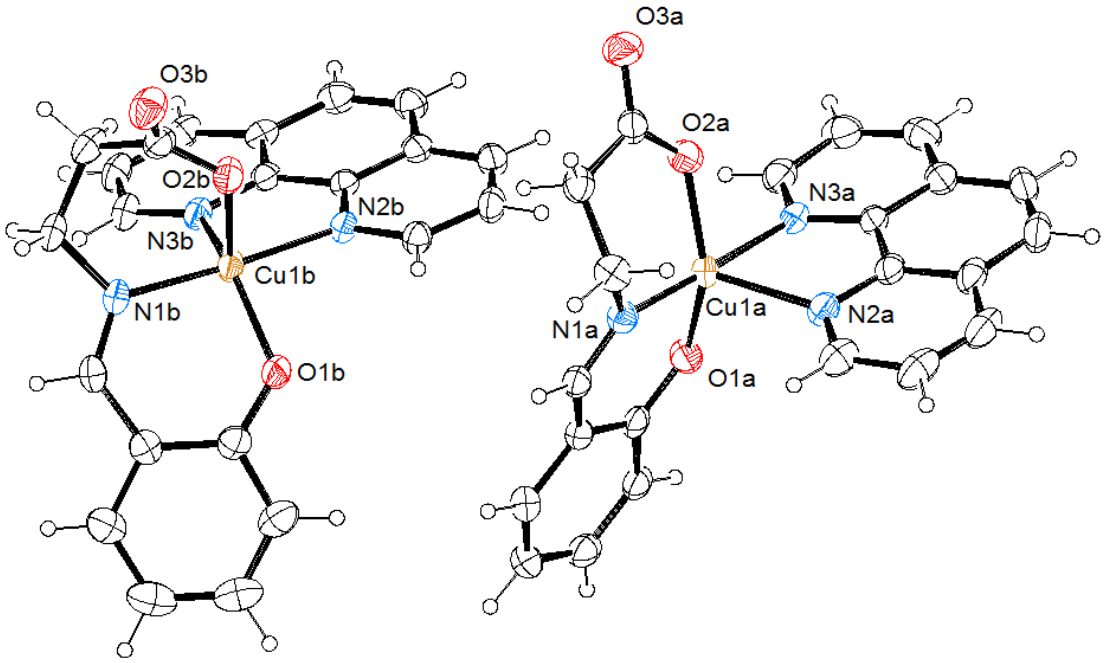
O3a
O3b
O2a
O2b
N3a
N2b
N3b
Cu1b
Cu1a
N1b
N2a
N1a
O1b
O1a

Fig.1

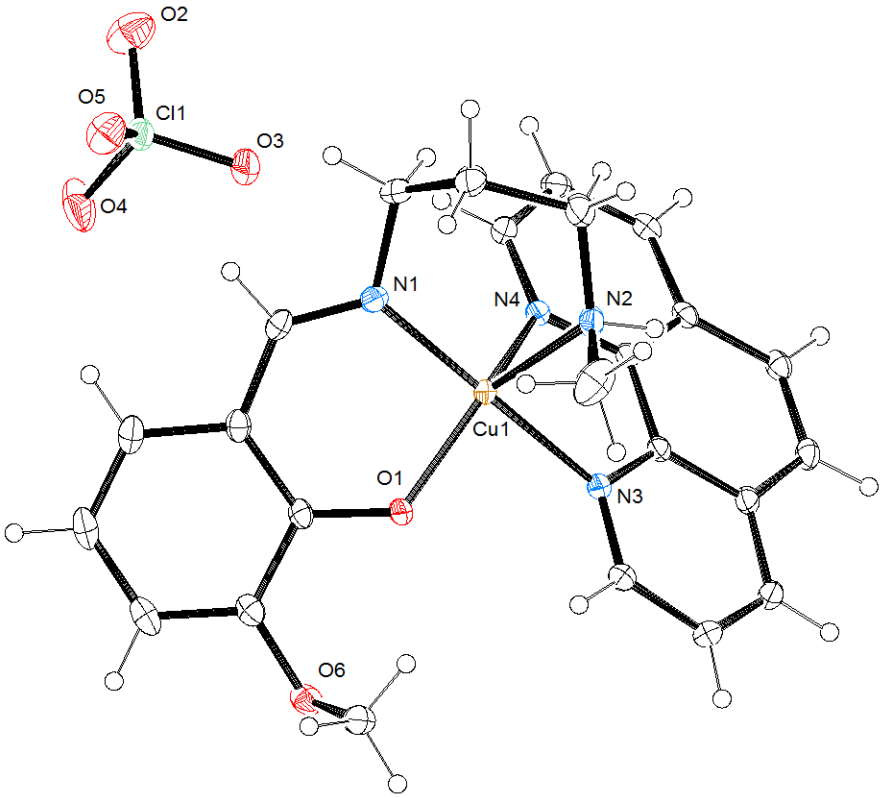
O2
O5
Cl1
O3
O4
N1
N4
N2
Cu1
O1
N3
O6

Fig.2

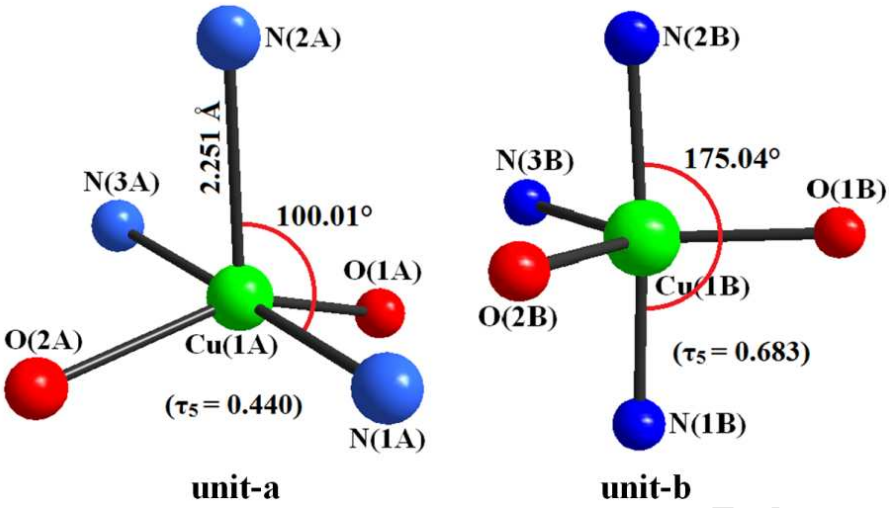
N(2A)
2.251 Å
N(3A)
100.01°
O(1A)
O(2A)
Cu(1A)
(τ5 = 0.440)
N(1A)
unit-a
N(2B)
N(3B)
175.04°
O(1B)
Cu(1B)
O(2B)
(τ5 = 0.683)
N(1B)
unit-b

Fig.3

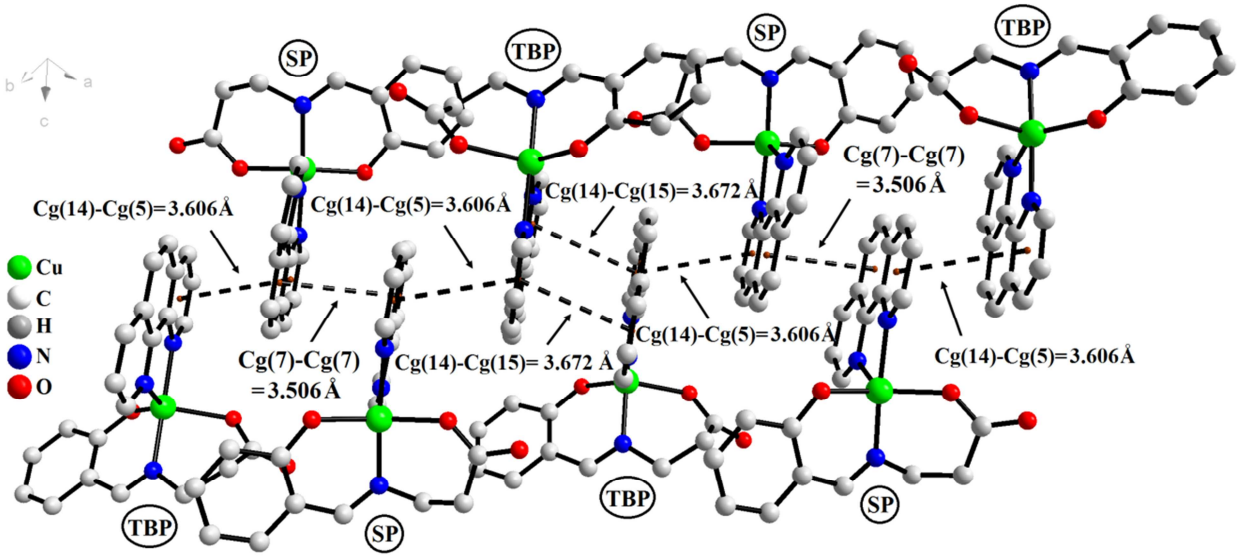
SP
TBP
SP
TBP
Cg(14)-Cg(5)=3.606Å
Cg(14)-Cg(5)=3.606Å
Cg(14)-Cg(15)=3.672 Å
Cg(7)-Cg(7)
=3.506 Å
Cu
C
H
N
O
Cg(7)-Cg(7)
=3.506 Å
Cg(14)-Cg(15)= 3.672 Å
Cg(14)-Cg(5)=3.606Å
Cg(14)-Cg(5)=3.606Å
TBP
SP
TBP
SP

Fig.4

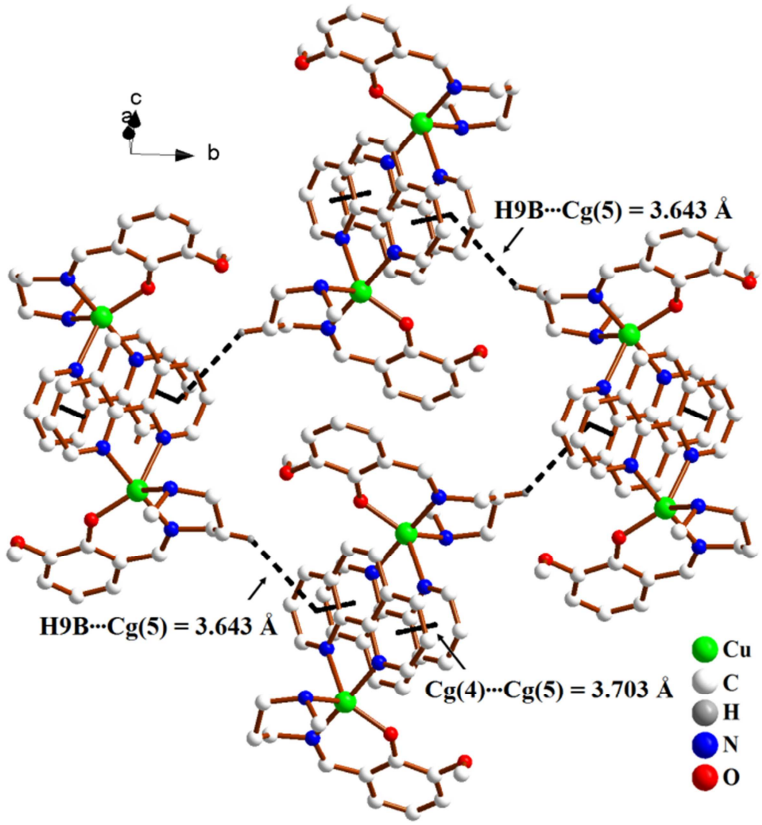
c
a
b
H9B···Cg(5) = 3.643 Å
H9B···Cg(5) = 3.643 Å
Cg(4)···Cg(5) = 3.703 Å
Cu
C
H
N
O

Fig. 5

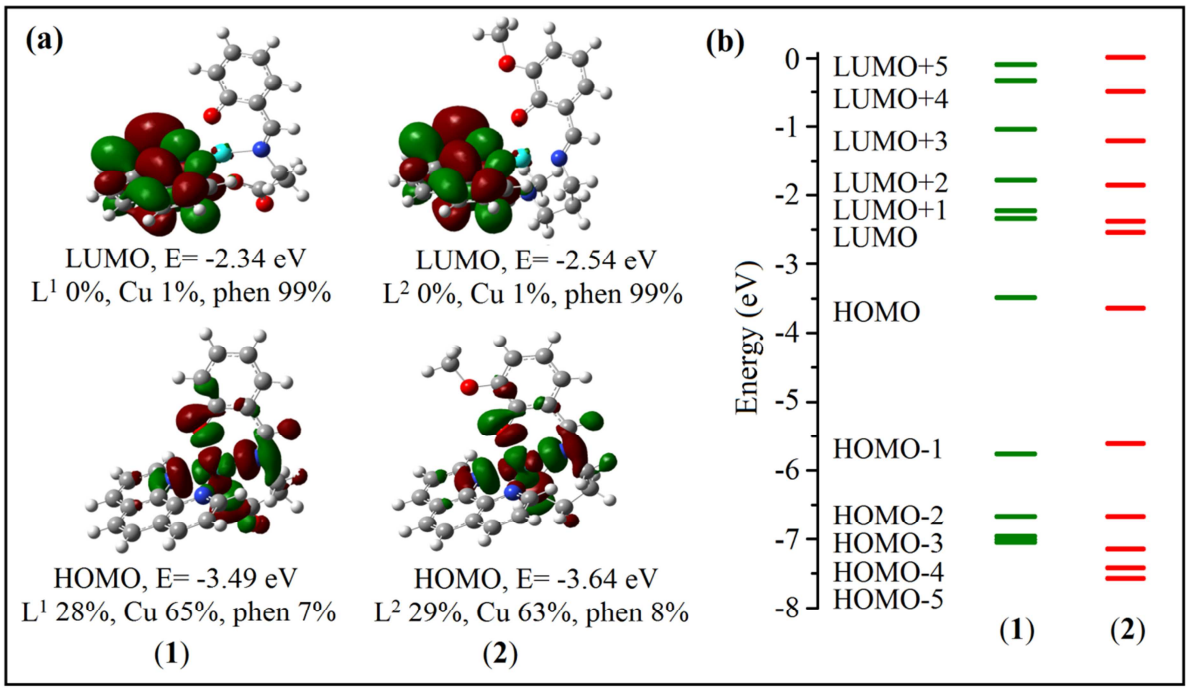
(a)
LUMO, E= -2.34 eV
L¹ 0%, Cu 1%, phen 99%
LUMO, E= -2.54 eV
L² 0%, Cu 1%, phen 99%
HOMO, E= -3.49 eV
L¹ 28%, Cu 65%, phen 7%
HOMO, E= -3.64 eV
L² 29%, Cu 63%, phen 8%
(1)
(2)
(b)
Energy (eV)
0
-1
-2
-3
-4
-5
-6
-7
-8
LUMO+5
LUMO+4
LUMO+3
LUMO+2
LUMO+1
LUMO
HOMO
HOMO-1
HOMO-2
HOMO-3
HOMO-4
HOMO-5
(1)
(2)

Fig. 6

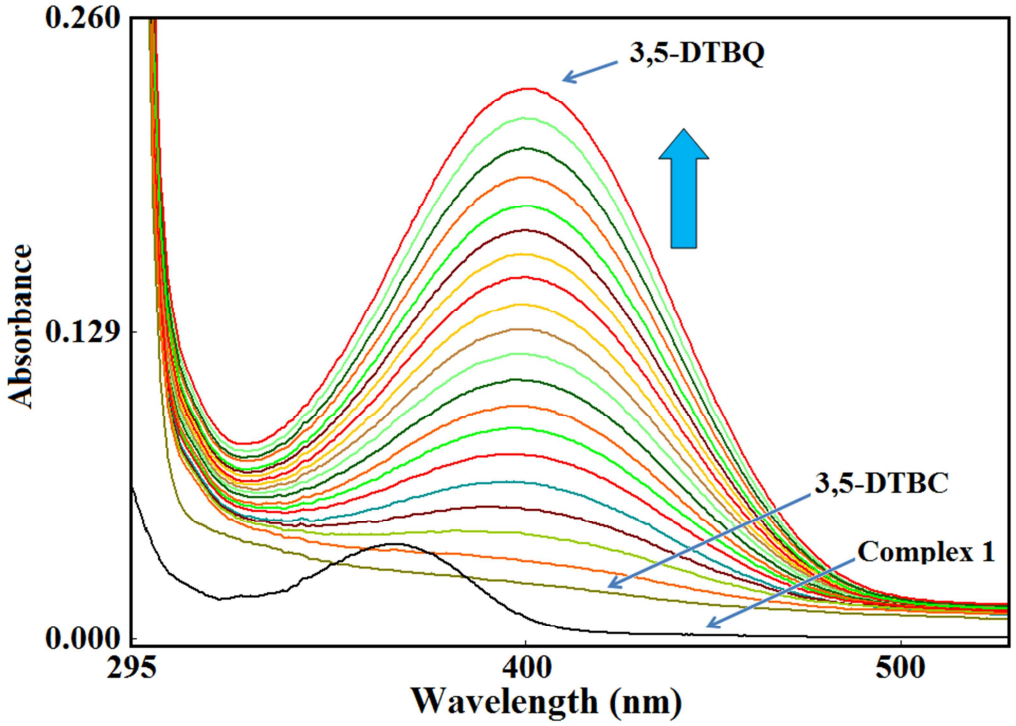
0.260
0.129
0.000
Absorbance
295
400
500
Wavelength (nm)
3,5-DTBQ
3,5-DTBC
Complex 1

Fig. 7

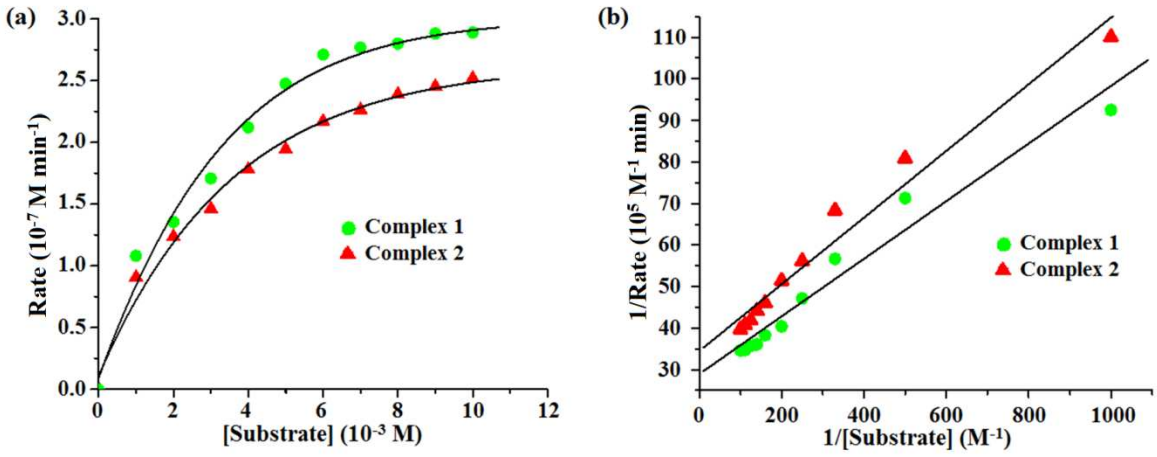
(a)
Rate (10⁻⁷ M min⁻¹)
[Substrate] (10⁻³ M)
Complex 1
Complex 2
(b)
1/Rate (10⁵ M⁻¹ min)
1/[Substrate] (M⁻¹)
Complex 1
Complex 2

Fig. 8

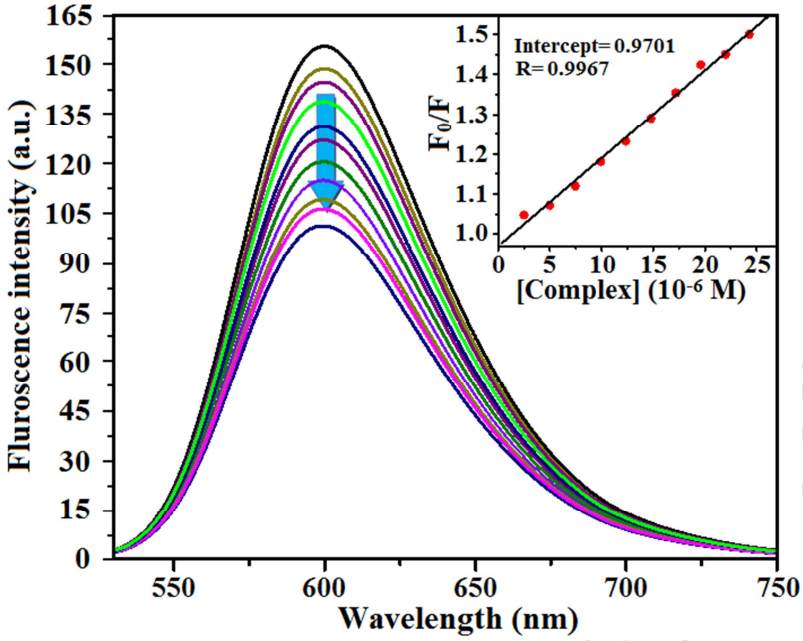

Fig. 9

Highlights

- Two five coordinated copper(II) complexes have been synthesized and characterized.
- Complexes form supramolecular structures with CH…π interactions.
- DFT/TD-DFT calculations have been performed.
- Complexes show catecholase activity.
- Spectroscopic studies reveal interaction of complexes with DNA.